

<https://doi.org/10.1038/s42005-024-01598-6>

Nanoscale precision brings experimental metalens efficiencies on par with theoretical promises

Check for updates

Villads Egede Johansen ¹, Uğur Meriç Gür ¹, Jade Martínez-Llinás ¹, Jesper Fly Hansen ¹, Akbar Samadi ¹, Maria Skak Vestergaard Larsen ¹, Theodor Nielsen ¹, Fredrik Mattinson ¹, Moritz Schmidlin ¹, N. Asger Mortensen ^{1,2,3} & Ulrich J. Quaade ¹ ✉

Metalenses are flat lenses, where sub-wavelength, so-called meta-atoms manipulate the electric field to perform a given lens function. Compared to traditional lenses, the two main drawbacks of metalenses are their achromatic limitations and low efficiencies. While an abundance of simulations show that efficiencies above 90% are attainable for low numerical apertures (NA), experimental reports showing such high efficiencies are limited. Here, we use electron-beam lithography (EBL) to realize a set of lenses with varying NA from 0.08 to 0.93. The low NAs were expected to fit the model, and the higher NAs determine the validity range of the model. We find that measured efficiencies above 92% for NA = 0.24 are achievable, and that a slight modification of the simulation model extends its validity to NA = 0.6. Based on our results, we discuss that the lower efficiencies reported in the literature are caused by low-fidelity manufacturing, closing the efficiency gap between measurements and simulation in metalens fabrication.

Metalenses are flat lenses, where the deflection of light is governed by a local electric field manipulation induced by so-called meta-atoms of three-dimensional (3D) sub-wavelength nanostructures¹. They normally consist of a flat sub-mm thick substrate, e.g. glass, deposited with a micron or sub-micron thick active layer, e.g. silicon (Si), containing the meta-atoms. Since the local field manipulation is determined by meta-atoms rather than the curvature of a homogeneous glass material in a traditional lens, almost arbitrary phase functions are easily implemented. Metalenses also bend light efficiently at high angles^{2,3}, which allows, for example, lenses with higher numerical aperture (NA) and thus lower f -number than refractive or multilevel diffractive lenses⁴.

Metalenses suffer two main drawbacks. First, metalenses have strong chromatic dispersion due to their diffractive nature. This has been addressed in a number of studies and polychromatic and achromatic lenses have been demonstrated, albeit at the loss of efficiency^{5,6}. Second, metalens efficiencies (rarely exceeding 90%⁷) are lower than for standard coated refractive lenses (close to 100%). These challenges limit the practical application of metalenses, and quoting Arbabi and Faraon: *...further increasing their efficiencies is essential for their applications in metasystems employing multiple cascaded metalenses*⁷. For many applications⁸ – such as 3D sensing, light detection

and ranging (LIDAR), optical communication, and laser-based head-up display – high efficiency is often required since it reduces unwanted scattering (in a lossless system), thus reducing stray light. The benefits from an efficiency increase are therefore twofold, since both higher efficiency and lower stray light increase the signal-to-noise ratio.

Efficiency is one of the most important figures-of-merits for metalenses, and multiple definitions exist, which complicates direct comparison to the literature^{9,10}. In this study, we deliberately use absolute focusing efficiency (FE) as our unambiguous efficiency merit, which is a suggestion of standardisation from Engelberg and Levy^{9,10}.

Our study focuses on narrow-band metalenses for the near-infrared region (NIR). We use a 940 nm wavelength model system to investigate (1) achievable FE for metalenses and; (2) the validity of the common meta-surface design approach, where each meta-atom represents a constant phase. This was performed by an experimental parameter study of metalenses with varying NA from low (NA = 0.08) to high (NA = 0.93). We expected the low-NA metalenses to be of high efficiency due to their spatially slow phase variation, whereas the large-NA metalenses were expected to perform worse due to their rapid phase variation. This is because the standard meta-atom model uses a locally periodic approximation

¹NIL Technology ApS, Haldor Topsøes Allé 1, DK-2800 Kongens Lyngby, Denmark. ²POLIMA–Center for Polariton-driven Light–Matter Interactions, University of Southern Denmark, Campusvej 55, DK-5230 Odense M, Denmark. ³Danish Institute for Advanced Study, University of Southern Denmark, Campusvej 55, DK-5230 Odense M, Denmark. ✉e-mail: uq@nilt.com

facilitating the use of periodic boundary conditions¹¹, i.e. a slow variation in meta-atom sizes. In order to obtain reliable results with high efficiency, we paid attention to the quality of manufacturing and investigated tolerances on the meta-atom level. The apparent efficiency gap between theoretical/computational predictions and experimentally realized efficiencies is a formidable challenge that calls for attention to the tight tolerances required for metalens manufacturing. We, therefore, summarise experimental results from the literature and show that our systematic manufacturing efforts lead to record-high efficiencies across the whole NA range, which are systematically better or on par with reports in the literature, and by this closing the gap.

Results

High focusing efficiency metalenses designed with low to high NA

In order to understand how to make high FE metalenses, we performed a parametric study of metalenses with constant diameter, $d_{\text{ens}} = 2.5$ mm, and varying focal lengths $f_d = \{14.925, 7.348, 4.770, 3.437, 2.598, 2.000, 1.530, 1.125, 0.726, 0.493\}$ mm. Using the beam diameter in our experimental setup ($d_{\text{beam}} = 2.4 \pm 0.1$ mm), this translates to $\text{NA} = \{0.08, 0.16, 0.24, 0.33, 0.42, 0.51, 0.62, 0.73, 0.86, 0.93\}$. We used the common approach of generating a library of meta-atoms with different phase shifts, obtained by simulating a uniform lattice of a given meta-atom using periodic boundary conditions (PBC)^{12,13}. For low NA, there is a slow variation of the phase-function, and the locally periodic approximation is therefore valid, leading to accurate FE predictions by assuming the meta-atom represents a constant phase and amplitude, and then propagating the phase field to the far field, for example by using the angular-spectrum method (ASM)¹⁴. This method is what we call the constant-phase approximation (CPA). For higher NA the approximation is challenged, and we investigate when this occurs and how it affects FE predictions. Due to the diffractive behaviour of the lenses¹⁵, the PSF is mainly governed by the lateral layout of the lens, and we did not expect any noticeable PSF degradation, since the lateral tolerances in our EBL are negligible in this respect⁷.

The highest diffraction limited FE for a metalens at normal incidence illumination is achieved by designs based on the following analytical phase function for a diffractive parabolic lens¹⁶

$$\phi(r) = -\frac{2\pi}{\lambda} \left(\sqrt{f_d^2 + r^2} - f_d \right), \quad (1)$$

which is measured in radians, λ is the free-space wavelength of the source, f_d is the focal length, and r is the radial distance from the center of the lens. This phase function has little practical application, but is widely used in the literature for benchmarking⁵. It was implemented with the meta-atoms in Fig. 1a, using anti-reflective coating (ARC) on the backside of the substrate to avoid reflections. Scanning-electron micrograph and optical micrograph

of one of the lenses are shown in Fig. 1b–c respectively. The metalens design based on truncated waveguides² is deliberately exploited to facilitate comparison to existing results in the literature^{17–28}.

The lenses were manufactured using EBL and reactive ion etching (RIE). From experience, we expected the standard deviation on pillar diameters to be around 2 nm from the nominal design, and atomic-force microscopy (AFM) confirms this level of side-wall and surface roughness (Supplementary Figs. 10–11 and Supplementary Table 7). The combination of phase function, ARC and tight tolerances enables gauging the highest possible FE we can obtain using a standard metalens design approach. Our nanofabrication efforts—with low roughness and accurate control of pillar dimensions and locations—reduce undesired scattering among diffraction orders that would otherwise affect the efficiency of the nominal design.

Modelling beyond the constant-phase approximation and experimental validation

The FEs were measured using the optical setup shown in Fig. 2c and described in Methods. We paid particular attention to calibration of the measured power onto the sample, since this is crucial for correctly assessing the FE.

The highest FEs were measured as 91.3% and 91.6% for $\text{NA} = 0.16$ and 0.24, respectively (Fig. 2a and Supplementary Table 1). Since we expected the $\text{NA} = 0.16$ lens to have the highest FE, we measured different realisations of the same lens across different wafers and measurement configurations, where we consistently obtained FEs in the range of 91–94% (Supplementary Table 3). This gives an indication of performance across wafers and measurement uncertainties, and since 91.3% is at the lower end of the interval, it confirms the consistency and reproducibility of the FEs.

We also predicted the FE using CPA, where we paid attention to mimicking the measurement conditions (see “Methods”). We observed simulated efficiencies of 90–94% for most NAs, which only offers a rough qualitative agreement with the experimental data points, while not capturing the declining trend for high NA (Fig. 2a). We conclude therefore that CPA gives reasonable results only up until $\text{NA} = 0.2$.

We also recorded PSFs for all lenses and calculated their modulation transfer functions (MTFs) as well as the Strehl ratio and non-normal incidence response (Fig. 2b, Supplementary Figs. 1–5 in Supplementary Note 1). Again, for low NA, there is a good match between model and simulation, with larger discrepancies for higher NAs.

In order to improve predictions beyond CPA, we next discretized each meta-atom unit cell into a 5×5 pixel representation of the field, thereby better representing the weakly inhomogeneous electric field across the unit cell. This increases the memory requirements and we therefore limited the simulations to down-scaled lenses with equivalent NAs. We refer to this as our resolved-field approximation (RFA), which captured the high-NA efficiency decline, offering a good quantitative agreement with measurements up to at least $\text{NA} \approx 0.6$. Both methods are local periodic

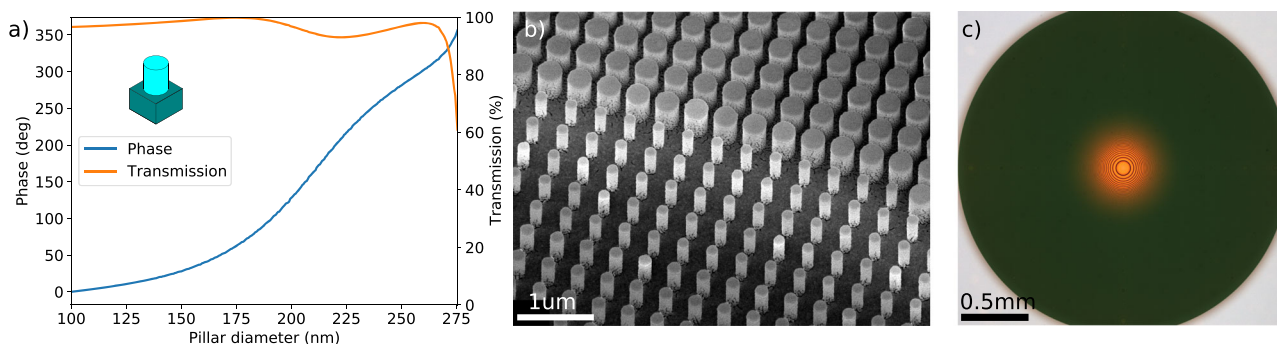


Fig. 1 | Metalens design. **a** The meta-atoms for the lenses consist of 500 nm tall cylindrical a-Si pillars on glass situated in a 400 nm square lattice. The dependence of phase (blue line, left-hand axis) and transmission (orange line, right-hand axis) on pillar diameter are based on electrodynamic simulations. All lenses were designed by

translating the phase function in Eq. (1) into pillar diameters on a lattice using this relation. **b** Scanning-electron microscope (SEM) image of a manufactured lens. **c** Optical micrograph of a manufactured lens.

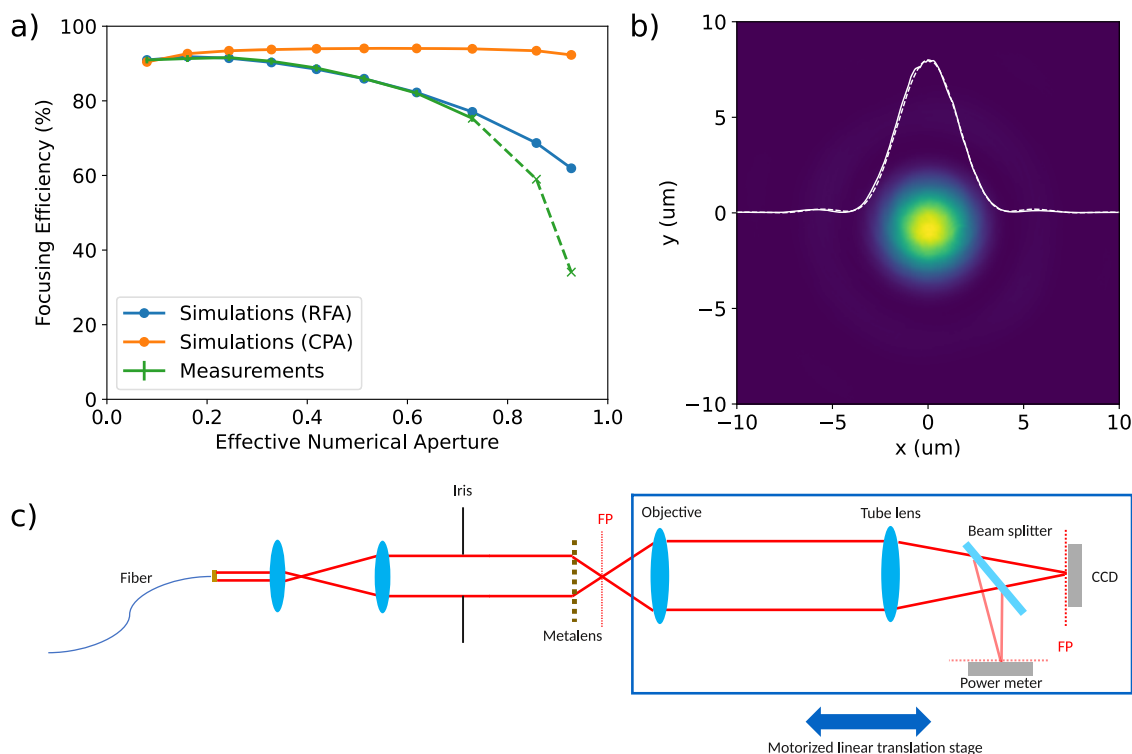


Fig. 2 | Focusing efficiency measurements and simulations. **a** Simulated (blue and orange lines with circles) and measured (green line) focusing efficiency (FE) versus the effective numerical aperture (NA). The dashed green line indicates the range where the NA of the lens is larger than the NA of the detector, thus not recording the full FE. The low-NA regime is qualitatively well-simulated by assuming each meta-atom emits a constant phase (constant phase approximation — CPA), while quantitative agreement is also obtained for a higher-NA regime when resolving the E -field above the meta-atoms on a grid (resolved field approximation — RFA). Raw data in Supplementary Table 1. The error bars (on top of round markers) show the standard deviation of repeated measurements as given in Supplementary Table 3 and are omitted for dashed data points due to known underestimation. **b** Measured

spread function (PSF) for NA = 0.16, with normalised cross-sections of simulated (dashed line) and measured (solid line) data. A tight fit between model and simulations is always expected for metalenses, where the lateral dimensions are controlled. **c** Schematic of the optical setup for metalens characterization, used for both PSF imaging and focusing efficiency measurements. The metalens is illuminated with a fiber delivery collimated laser. An open microscope mounted on a motorized stage and equipped with a camera and a power meter located at the focal plane (FP) of the tube lens is used to image the PSF on a charge-coupled device (CCD) camera and collect the optical power from the FP of the metalens to measure the focusing efficiency.

approximations based on the same principle. A discussion of more advanced approaches is found in Ref. 11. The improved fit suggests that RFA has a wider range of applicability than CPA for predicting lens FEs.

High focusing efficiency enabled through precise manufacturing

From the FE measurements, we obtain up to 92% efficiency (Fig. 2a), and the range up to NA=0.33 even stays above 90%. Our choices of design method, design wavelength, meta-atom geometry and optical materials are commercially relevant and common choices in the literature. Our definition of FE is furthermore a conservative choice that normally gives the lowest value (as opposed to e.g. diffraction and transmission efficiencies or other relative definitions used in the literature)^{9,10}. We therefore ascribe the superior FE compared to earlier reports (and own early-stage unpublished results), even when corrected for ARC, to the precise control of our manufacturing process (pillar diameter tolerances, side-wall profile, and roughness) and material choices (refractive index, purity, roughness, layer height). To demonstrate the importance of precision, we have simulated the effect on the efficiency of a constant offset on meta-atoms diameter, which shows that the tolerances need to be within roughly ± 5 nm from the target values to avoid a noticeable decline in FE (Fig. 3a, c). Considering the tight fit to the ideal simulated values, the knowledge of manufacturing precision, and the tight tolerances extracted from the tolerance study, we conclude that the manufactured lenses are closely replicating even the nanoscale aspects of the nominal lens designs, which in turn explains the high measured efficiencies.

Lacking nanoscale precision leads to simulation-efficiency gap

Since our measured FEs seemed to exceed values reported in the literature for comparable NAs, we searched the literature for experimental FEs to check if this is the case (Fig. 4 and Supplementary Tables 8–10 in Supplementary Note 4). We used a catch-all method, where we recorded focusing efficiencies and NAs without differentiating focusing efficiency definition; lens phase function; or wavelength, which we however limited to VIS, NIR, and SWIR.

We took a closer look at the three outliers: For Ref. 26, there is no clear definition of focusing efficiency, since it is claimed that the reference is also measured at focus position – but without lens, there is no focus, and it is also unclear if the reference power is also passing through the substrate. However, the measurement might be comparable and would in that case indicate good manufacturing. For Ref. 27, it is unclear if they calibrate out the substrate when measuring the reference, but since they do not have anti-reflective coating on the back, their measurements might be comparable to our definition and indicate good manufacturing. For Ref. 21, we are unsure how they can measure such high efficiency (NA = 0.6, FE = 90%) when using a meta-atom-based approach, even when correcting for their reference power being measured through the substrate, and we have not been able to reproduce their efficiencies when simulating that lens.

From this investigation, we conclude that our simulated and measured values are representative of a systematic upper boundary for lens efficiency when using the standard meta-atom-based approach (but should be adjusted through simulation for different materials, wavelengths, lattices, etc.). We are aware that the study does not cover every metalens publication

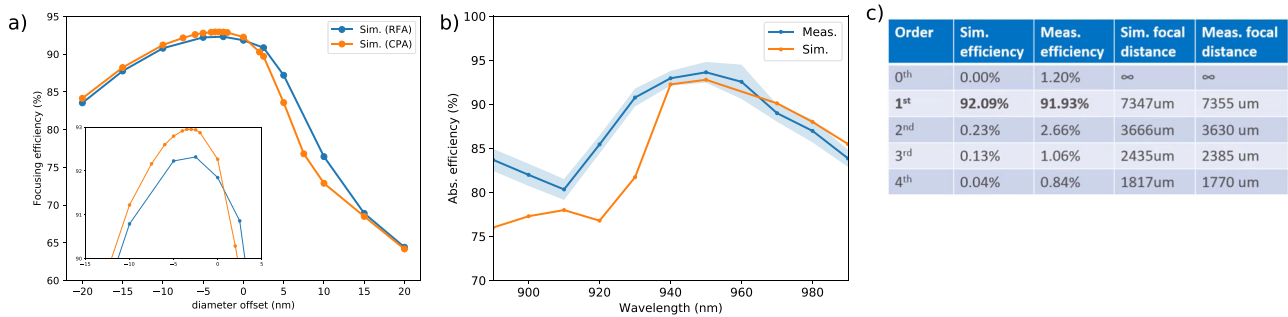


Fig. 3 | Metalens tolerances and detailed characterisation. The numerical aperture NA = 0.16 lens was investigated in detail: (a) Simulation study (resolved field approximation (RFA): blue circles, constant phase approximation (CPA): orange circles) showing the effect on FE when the meta-atom diameters are uniformly offset compared to their target value. For variations larger than $\sim \pm 5$ nm from the target diameters, the focusing efficiency (FE) drops below 90%. CPA and RFA give similar results for this low-NA simulation. **b** Measured and simulated FE compared to

wavelength (blue and orange circles, respectively), showing a ~ 35 nm bandwidth, where the FE stays above 90%. Raw data is in Supplementary Table 2. The shading indicates the error bars that show the standard deviation from three consecutive measurements at each wavelength. There is a quantitative discrepancy between measured and predicted efficiencies, but the same trends are captured in both graphs. **c** Higher order efficiency measurements for the NA = 0.16 lens.

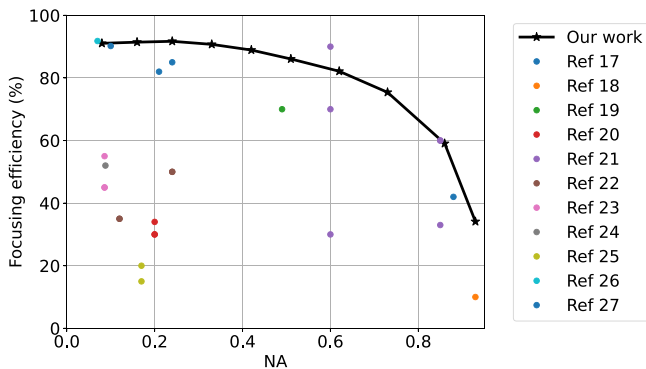


Fig. 4 | Reported lens focusing efficiencies from the literature. The coloured dots visualise focusing efficiencies (no matter definition) for different NAs reported in the literature^{17–27}. The measurements from this paper are included (black stars, error bars in Fig. 2). Not all lenses might be designed for monochromatic focusing, which could explain their lower efficiency, but in general we observe no values, apart from one data point, exceeding the values in this article, where we have ensured tight tolerances during manufacturing.

in the literature (there are simply too many) but we made sure to include often-cited publications since we assumed we would be more likely to find high-efficiency reports there. We were also not able to find a review article summarising efficiencies, but we did check reviews that reported efficiencies to ensure that we had not overlooked high-efficiency lenses found there⁵. Our measurements and simulations do not represent an upper physical limit for efficiency, rather they represent the limit for polarisation-insensitive meta-atom/CPA-based designs, which covers most manufactured lenses reported in the literature. From this analysis, we therefore hypothesize that there is a simulation-efficiency gap caused by the lack of attention to the nanoscale precision required when fabricating metalenses.

Other transmission and reflection orders account for lost efficiency

In order to account for the remaining power not reaching the focal point, we decided to measure the power of the ballistic light/zero order as well as the power in several higher-order transmission and reflection focal points for the NA = 0.16 lens. We used a 50:50 beam splitter for illumination in this configuration (see “Methods”, Supplementary Note 2, and Supplementary Fig. 6). By doing so, we get an almost complete overview of how the lens redistributes the electromagnetic energy. Energy conservation furthermore serves as a sanity check of the experimental setup, by ensuring that the sum

of energies is less than 100%. The reflected orders for this lens were all below the noise floor (0.1% relative to the lens’ FE), and the measured transmission orders are presented in Fig. 3. For comparison, reflection measurements above the noise floor for a lens with lower efficiency are presented in Supplementary Table 6. By summing the lower orders in Fig. 3, we find that we account for 97.7% of the energy in the system, and we expect the rest of the energy distributed between stray light, small losses, other orders, and measurement uncertainty. We are therefore capable of ensuring the quality of our measurements as well as mapping the re-distribution of light for our lenses. We measured the first three transmission orders for all lenses (Supplementary Tables 4–5), observing that the amount of energy going to the higher orders is not strictly correlated with the 1st order efficiency. This suggests that more light is reflected for higher NA.

To further corroborate the quality of the lenses against the experimental validation and simulations, we investigate the wavelength dependence of the FE. This was done experimentally by tuning the wavelength of the light source as well as finding a new optimal focal distance. For the simulations, it meant re-calculating the meta-atom library at different wavelengths for subsequent input to the phase field generation (Fig. 3b). It can be seen that all trends from the measurements are replicated, albeit not fully quantitatively reproduced by the simulations. The good fit between measurements and simulations shows the robustness of our approach. It furthermore shows how a chromatic-designed metalens retains its high focusing efficiency for a certain wavelength range. This is important from a commercial perspective because even for laser-based imaging, the wavelength might drift, especially due to temperature changes and fluctuations.

Manufacturing quality directly affects image quality

Lack of nanoscale precision during manufacturing will degrade image performance in practical applications. As an example, we compare the image quality of two seemingly similar imaging lenses based on the same design but manufactured with different fidelity. The system is described in detail by Mattinson et al.²⁹ and is a similar configuration to Ref. 30. The camera setup of the experiment is shown in Fig. 5a. The two lenses tested in the system have on-axis FEs of 58% and 85% respectively. The phase function $\phi(r) = -2685 \cdot \left(\frac{r}{1\text{mm}}\right)^2$ is designed for imaging, meaning that only the central part will contribute to an on-axis focal spot, and values are thus not directly comparable with Eq. (1). When comparing Fig. 5b and c, we note a visible increase in brightness due to the increased efficiency, but furthermore, we notice a bright spot in the center of Fig. 5b and absent in Fig. 5c. This is a defocused image caused by the stray light directed by the 2nd order lens function^{7,15,29}. In general, the lower efficiency in the 1st order, the more energy in other orders, and this is why we see the bright spot effect. The 2nd order focal point is closer to the lens than the 1st order, and

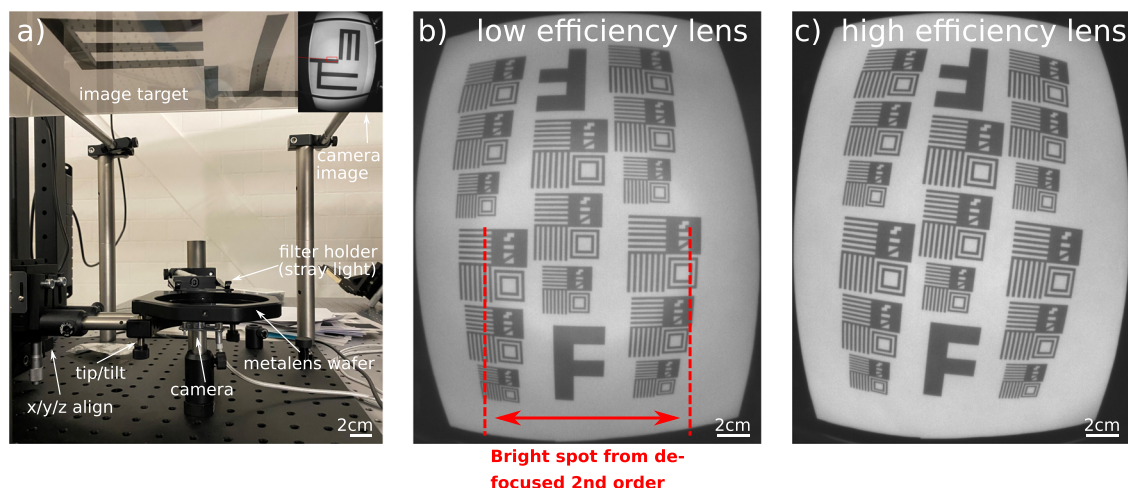


Fig. 5 | Two metalenses with different nanoscale precision. **a** Lab camera setup for showing the importance of metalens manufacturing. The 80° field of view metalens (containing an aperture on the backside of the substrate) is placed facing the camera sensor and manually adjusted to focus on the lens. The NA of the metalens is 0.31. The test target is illuminated from the back with a 940 nm diffused source. Scale bar accurate for central part of image. **b** Imaging of a test target using a metalens with 58% efficiency, meaning that higher order lensing is also non-negligible. The bright

spot indicated on the figure is the defocused image from the 2nd order lens. The scale bar is for the original target disregarding distortion. **c** Imaging using exactly the same lens design as in (b), but with higher nanoscale precision during manufacturing. This leads to higher 1st order efficiency (85%) and in turn both a brighter image and negligible contribution from the 2nd order lens function. Scale bar is for original target disregarding distortion.

therefore the contribution from the 2nd order is strongly defocused. This example illustrates just how important precise nanoscale manufacturing is.

Conclusion

We designed, manufactured, and measured a range of focusing metalenses for 940 nm with varying numerical aperture. The dual purpose was (1) to experimentally confirm a design-predicted 92% absolute focusing efficiency and; (2) to investigate the range of NA for which simple beam propagation, where each meta-atom represents a constant phase, could correctly predict the FE. The lenses were designed using the common method of interpolating a given lens phase function using a library of meta-atoms with varying pillars, where the phase was simulated using RCWA. We experimentally found FEs up to 92%, and for $NA \lesssim 0.33$ every lens FE exceeded 90%, followed by a declining trend in efficiency for higher-NA lenses, which is theoretically expected already from the nominal design of the lens. Even at $NA = 0.62$, we could still measure 82%. These results are among the highest experimental efficiencies reported for polarisation-insensitive lenses. The nanoscale precision and control in our manufacturing pipeline enables high efficiency. In particular, we show through simulations that a precision of roughly ± 5 nm on pillar diameters is required to avoid losing several percentage points or more in focusing efficiency.

Using CPA, we could predict FEs matching experiments up until $NA=0.16$. However, if we substituted CPA with RFA, we achieved a close fit up until $NA=0.6$. It is intriguing how just a slightly better electric field resolution greatly increased the validity of the model, even though the periodic assumption did not change. We expect the models to either overshoot or match realisable FEs due to their simplicity, which ignores effects that would normally lower FEs (coupling, tolerances, ...). The match between measurements and RFA model therefore suggests that manufacturing was so close to the nominal design that there was no efficiency potential from further process improvements.

The experimental study and simulation model are cross-validated by measuring wavelength dependence, higher-order focusing, reflection focusing, and ballistic light (zero order) for a selected lens. It is to our knowledge the first reported measurement setup also investigating reflected orders for transmission metalens and accounted for almost all the light redistributed by the metalens. Taken together, the measurements and simulations validate the high efficiencies we measure and give insight into

the required nanoscale precision as well as the validity of CPA and RFA for modelling.

Confidently knowing the expected experimental FEs for metalenses is critical for realising future metalens-based commercial³¹ and research applications. By this study, we present a guideline for FEs for a large range of NAs that closes the simulation-efficiency gap by adequate modelling and improved nanoscale manufacturing precision. We see this work as a benchmark to steer labs toward high-precision manufacturing, and subsequently as a baseline from which to improve. Several other design strategies exist³², and to go beyond the RFA model, we suggest introducing more degrees of freedom in meta-atom shape and location mixed with full-wave modelling as an enabler for higher efficiencies^{2,32,33}. This can be combined with an investigation into more complex topology-optimised shapes^{3,34}, possibly aided by large-scale topology optimisation problem^{11,35}. This includes considering other parameters such as angle, wavelength, and polarisation dependence. This will allow novel applications and bring metalenses to a new level of maturity.

Methods

Simulation – CPA, RFA

Our use of the constant phase approximation (CPA) – where each meta-atom is replaced by a constant amplitude and phase, found from the 0th order mode amplitude, and then propagated to the far-field – is probably the most widespread method for designing metalenses^{2,11,22}. Resolved field approximation (RFA) instead resolves the scalar E field (same polarisation) right on top of the meta-pillar in a low-resolution Cartesian point grid. For our case, we used 5×5 pixels. This means, that instead of representing the meta-atom with a 1-pixel electric field value, we use a 5×5 field representation.

Considering a surface of uniform meta-atoms, the two methods coincide in the far field since the subwavelength periodicity will only allow 0th order propagation, and any discretization of the field on the top of the structure would lead to the same mode efficiency. However, their near fields differ. If we now allow the meta-atoms to vary, then we also introduce more propagating modes to redistribute the light into, and the RFA better resolves this redistribution. It is worth re-stating, that both CPA and RFA rely on periodic boundary conditions (PBC), while our experimental results suggest that the RFA works for a larger NA-range.

In our implementation, all meta-atoms were simulated using a Python-implementation of the rigorous coupled-wave analysis (RCWA) of the electrodynamic response^{36,37}. This method exploits PBCs in the lateral dimensions, and extracts the phase and transmission properties from the complex-numbered zero-order transmission mode, which is the only propagating mode for the surface since the meta-atom lattice is subwavelength. It is then either assumed that this phase is constant throughout the lattice of the meta-atom (CPA) or resolved and sampled in different positions in the lattice (RFA). By doing this across the surface, a phase field is obtained. The overall metalens efficiency was determined by propagating the phase field to the focal point using an in-house implementation of the angular-spectrum method (ASM) similar to the one in Ref. 38. The energy in the focal point was then numerically integrated. To increase resolution, zero padding and/or upsampling of the design is used. The method with a constant-phase approximation is expected to be accurate for slow variations of the phase function, where the locally periodic approximation is valid, and where the slowly varying field is well-approximated by the scalar propagator. We therefore expect a decrease in accuracy for increasing NA. In contrast to CPA, as RFA resolves the field distribution, it gives better accuracy. For NAs larger than 0.7, the phase gradient rapidly increases, therefore the locally periodic approximation becomes invalid. Consequently, RFA suffers. While it provides a better representation of the physics, it requires more memory and computational time, and the amount of additional requirements depends on the ASM implementation being used.

Lens simulations

We used the RCWA meta-atom library to generate the phase field right at the lens when illuminated with a plane wave. First, we limited the size of the incident field in the simulation to a diameter of 2.4 mm to match the experimental illumination. We then propagated the light to the focal point with the ASM and integrated the energy in a disk of radius 45 μm centered around the optical axis to mimic the size of the detector in the experiment. For energy integrations, fields were oversampled until convergence was achieved.

Processing/fabrication

A 500 nm film of a-Si was sputter-coated on a D263T Eco glass substrate, and an ARC deposited on the backside of the substrate. The substrate was patterned using EBL (Raith EBPG5200) using resist (Zep520A, Zeon Corporation) and an electron discharge layer (Thermal Al, Wordentec QCL800). Subsequently the pattern polarity was inverted using a lift-off mask, and the a-Si was etched using fluorine chemistry (ICP RIE tool, SPTS), and the mask layer was removed using oxygen (O_2) plasma (300 Plasma Processor, TePla).

Mechanical and refractive index characterisation

The optical parameters of amorphous silicon were characterized using ellipsometry (Ellipsometer VASE – J. A. Woollam), where $n(940\text{ nm}) = 3.55$, and $k(940\text{ nm}) = 7 \times 10^4$. The pillar height was post-fabrication measured with atomic force microscopy (AFM) to 499 nm (Dimension Icon-PT – Bruker AXS). In Supplementary Note 3, there are figures providing details on mechanical characterisation. In Supplementary Fig. 9a, a top-down SEM of the structures is presented demonstrating the shape quality of the meta-atoms. In Supplementary Fig. 9b a tilted SEM is presented to demonstrate the sidewall profile of the meta atoms. Single meta-atoms were qualitatively analysed in Supplementary Fig. 9c, d.

Optical characterisation

Optical characterization of metalenses was carried out using the in-house custom setup shown in Fig. 2c. The setup consists of an illumination arm coupled with a 940 nm fiber delivery collimated supercontinuum laser (NKT Photonics, SuperK COMPACT, unpolarized TEM00 mode), and an open microscope (Objective lens; NA = 0.85, 100 \times Olympus LCPLN100XIR or NA = 0.7, 100 \times Mitutoyo WF255001919) equipped with a motorized stage (Thorlabs, LNR502E/M) as a detection arm. The

collimated beam was expanded by a factor of 5 (beam diameter about 5 mm) before passing through an iris for beam size adjustment on the metalens. The cross-section of the beam for an iris diameter of 2 mm can be seen in Supplementary Fig. 8. The focused beam from the metalens is characterized by means of measuring effective focal length (EFL), imaging PSF, and focusing efficiency measurements. The EFL of the metalens is obtained by measuring the distance between the planes of the metalens' surface and the PSF captured by the camera located at the focal plane of the tube lens. A beam splitter (BS) after the tube lens was used to split the image of PSF onto the camera and a power meter for PSF imaging and focusing efficiency measurements. Captured images of the focal spot are then analyzed to extract the PSF.

For focusing efficiency measurements, the optical power from the focal plane (FP) of the metalens is measured using a power meter (Thorlabs' C-Series Photodiode Power Meter Sensors, S120C) located at the FP of the tube lens. Hence the PSF power was measured at the focal plane of the tube lens (conjugate plane of metalens' FP), for focusing efficiency assessment, the incident beam also needed to be measured at the same plane (Supplementary Fig. 7). By removing the metalens from the light path as the incident collimated beam focuses on the back focal plane of the objective lens, it is not feasible to collect the incident beam at the focal plane of the tube lens. Thus, we have replaced the metalens with a slowly focusing refractive lens (Thorlabs AL2550M Aspheric Lens, $f = 50\text{ mm}$) for incident beam power measurement by directly measuring power at the focal plane of the refractive lens and measuring it at the focal plane of the tube lens to obtain the transmission factor of the microscope, relating the direct measurement of the incident beam to the power at the focal plane of the tube lens.

For the measurements in Fig. 2, an objective lens with NA = 0.85 was used, meaning that for metalenses with an NA larger than 0.85, we expect an underestimation of the FE. For the measurements in Fig. 3, an objective lens with NA = 0.7 was used.

Data availability

The data that underlie the findings of this study are available from the corresponding author upon reasonable request.

Received: 28 January 2024; Accepted: 13 March 2024;

Published online: 09 April 2024

References

1. Yu, N. & Capasso, F. Flat optics with designer metasurfaces. *Nat. Mater.* **13**, 139–150 (2014).
2. Byrnes, S. J., Lenef, A., Aieta, F. & Capasso, F. Designing large, high-efficiency, high-numerical-aperture, transmissive meta-lenses for visible light. *Optics Express* **24**, 5110–5124 (2016).
3. Sell, D., Yang, J., Doshay, S., Yang, R. & Fan, J. A. Large-angle, multifunctional metagratings based on freeform multimode geometries. *Nano Lett.* **17**, 3752–3757 (2017).
4. Engelberg, J. & Levy, U. The advantages of metalenses over diffractive lenses. *Nat. Commun.* **11**, 1991 (2020).
5. Chen, W. T., Zhu, A. Y. & Capasso, F. Flat optics with dispersion-engineered metasurfaces. *Nat. Mater.* **5**, 604–620 (2020).
6. Engelberg, J. & Levy, U. Achromatic flat lens performance limits. *Optica* **8**, 834–845 (2021).
7. Arbabi, A. & Faraon, A. Advances in optical metalenses. *Nat. Photon.* **17**, 16–25 (2023).
8. Neshev, D. N. & Miroshnichenko, A. E. Enabling smart vision with metasurfaces. *Nat. Photon.* **17**, 26–35 (2023).
9. Engelberg, J. & Levy, U. Standardizing flat lens characterization. *Nat. Photon.* **16**, 171–173 (2022).
10. Engelberg, J. & Levy, U. Generalized metric for broadband flat lens performance comparison. *Nanophotonics* **11**, 3559–3574 (2022).
11. Lin, Z. & Johnson, S. G. Overlapping domains for topology optimization of large-area metasurfaces. *Optics Express* **27**, 32445–32453 (2019).

12. Lalanne, P., Astilean, S., Chavel, P., Cambriil, E. & Launois, H. Design and fabrication of blazed binary diffractive elements with sampling periods smaller than the structural cutoff. *J. Opt. Soc. Am. A* **16**, 1143–1156 (1999).
13. Ding, F., Pors, A. & Bozhevolnyi, S. I. Gradient metasurfaces: a review of fundamentals and applications. *Rep. Progr. Phys.* **81**, 026401 (2017).
14. Goodman, J. W. *Introduction to Fourier Optics* (McGraw-Hill, 1996), 2nd edn.
15. O’Shea, D. C., Suleski, T. J., Kathman, A. D. & Prather, D. W. *Diffractive Optics: Design, Fabrication, and Test*, chap. 4: Diffractive Lens Design, 57–82 (SPIE, 2004).
16. Levy, U., Mendlovic, D. & Marom, E. Efficiency analysis of diffractive lenses. *J. Opt. Soc. Am. A* **18**, 86–93 (2001).
17. Arbabi, A., Horie, Y., Ball, A. J., Bagheri, M. & Faraon, A. Subwavelength-thick lenses with high numerical apertures and large efficiency based on high-contrast transmitarrays. *Nat. Commun.* **6**, 7069 (2015).
18. Paniagua-Domínguez, R. et al. A metalens with a near-unity numerical aperture. *Nano Lett.* **18**, 2124–2132 (2018).
19. Arbabi, A. et al. Miniature optical planar camera based on a wide-angle metasurface doublet corrected for monochromatic aberrations. *Nat. Commun.* **7**, 13682 (2016).
20. Chen, W. T., Zhu, A. Y., Sisler, J., Bharwani, Z. & Capasso, F. A broadband achromatic polarization-insensitive metalens consisting of anisotropic nanostructures. *Nat. Commun.* **10**, 355 (2019).
21. Khorasaninejad, M. et al. Polarization-insensitive metalenses at visible wavelengths. *Nano Lett.* **16**, 7229–7234 (2016).
22. Shrestha, S., Overvig, A. C., Lu, M., Stein, A. & Yu, N. Broadband achromatic dielectric metalenses. *Light Sci. Appl.* **7**, 85 (2018).
23. Fan, Z.-B. et al. A broadband achromatic metalens array for integral imaging in the visible. *Light Sci. Appl.* **8**, 67 (2019).
24. Zhang, S. et al. Solid-immersion metalenses for infrared focal plane arrays. *Appl. Phys. Lett.* **113**, 111104 (2018).
25. Ye, M., Ray, V. & Yi, Y. S. Achromatic flat subwavelength grating lens over whole visible bandwidths. *IEEE Photon. Technol. Lett.* **30**, 955–958 (2018).
26. She, A., Zhang, S., Shian, S., Clarke, D. R. & Capasso, F. Large area metalenses: design, characterization, and mass manufacturing. *Optics Express* **26**, 1573–1585 (2018).
27. Wang, Y. et al. High-efficiency broadband achromatic metalens for near-ir biological imaging window. *Nat. Commun.* **12**, 5560 (2021).
28. Decker, M. et al. Imaging performance of polarization-insensitive metalenses. *ACS Photon.* **6**, 1493–1499 (2019).
29. Mattinson, F. et al. Latest advancements at NILT on flat metalens based camera modules in near infrared. *Proc. SPIE* **12217**, 1221707 (2022).
30. Engelberg, J. et al. Near-ir wide-field-of-view huygens metalens for outdoor imaging applications. *Nanophotonics* **9**, 361–370 (2020).
31. Pitruzzello, G. Metaoptics for the consumer market. *Nat. Photon.* **17**, 6–7 (2022).
32. So, S., Mun, J., Park, J. & Rho, J. Revisiting the design strategies for metasurfaces: fundamental physics, optimization, and beyond. *Adv. Mater.* **35**, 2206399 (2023).
33. Phan, T. et al. High-efficiency, large-area, topology-optimized metasurfaces. *Light Sci. Appl.* **8**, 8 (2019).
34. Wang, E. W., Sell, D., Phan, T. & Fan, J. A. Robust design of topology-optimized metasurfaces. *Opt. Mater. Express* **9**, 469–482 (2019).
35. Chung, H. & Miller, O. D. High-na achromatic metalenses by inverse design. *Optics Express* **28**, 6945–6965 (2020).
36. Liu, V. & Fan, S. S⁴: a free electromagnetic solver for layered periodic structures. *Comp. Phys. Commun.* **183**, 2233–2244 (2012).
37. Jin, W. Multiple z for fieldongrid github.com/weiliangjinca/grcwa (2021).
38. Fuente, R. Simulating diffraction patterns with the angular spectrum method and python [github.com/rafael-fuente/Diffraction-Simulations—Angular-Spectrum-Method](https://github.com/rafael-fuente/Diffraction-Simulations-Angular-Spectrum-Method) (2018).

Acknowledgements

The authors thank Lars Hagedorn Frandsen and Sif Fugger for technical assistance, and Uriel Levy for stimulating discussions on efficiency measures for metalenses. N.A.M. is a VILLUM Investigator supported by VILLUM FONDEN (grant No. 16498) and the Danish National Research Foundation (Project No. DNRF165).

Author contributions

V.E.J., U.J.Q., and T.N. designed the experiment. V.E.J., U.M.G., and J.M.-L. designed the structures and simulated the electromagnetic properties. U.M.G. and J.M.L. performed a literature study. J.F.H. fabricated the structures and performed the scanning electron microscopy. J.F.H. performed ellipsometry. A.S. and M.S.V.L. performed the optical measurements. F.M. designed the imaging lens. M.S. build imaging lens characterisation and camera setup. V.E.J., N.A.M., and U.J.Q. supervised the project. All authors contributed to the discussion and interpretation of the results, and the writing of the manuscript was done in a joint effort.

Competing interests

The authors declare no competing interests.

Additional information

Supplementary information The online version contains supplementary material available at <https://doi.org/10.1038/s42005-024-01598-6>.

Correspondence and requests for materials should be addressed to Ulrich J. Quaade.

Peer review information This manuscript has been previously reviewed in another Nature Portfolio journal. The manuscript was considered suitable for publication without further review at *Communications Physics*.

Reprints and permissions information is available at <http://www.nature.com/reprints>

Publisher’s note Springer Nature remains neutral with regard to jurisdictional claims in published maps and institutional affiliations.

Open Access This article is licensed under a Creative Commons Attribution 4.0 International License, which permits use, sharing, adaptation, distribution and reproduction in any medium or format, as long as you give appropriate credit to the original author(s) and the source, provide a link to the Creative Commons licence, and indicate if changes were made. The images or other third party material in this article are included in the article’s Creative Commons licence, unless indicated otherwise in a credit line to the material. If material is not included in the article’s Creative Commons licence and your intended use is not permitted by statutory regulation or exceeds the permitted use, you will need to obtain permission directly from the copyright holder. To view a copy of this licence, visit <http://creativecommons.org/licenses/by/4.0/>.

© The Author(s) 2024